Multiatomic mirror for perfect reflection of single photons in a wide band of frequency

Yue Chang (常越), Z. R. Gong (龚志瑞),* and C. P. Sun (孙昌璞)†
Institute of Theoretical Physics, Chinese Academy of Sciences, Beijing 100190, China

(Received 26 May 2010; revised manuscript received 17 December 2010; published 31 January 2011)

A resonant two-level atom doped in a one-dimensional waveguide behaves as a mirror, but this single-atom "mirror" can only reflect single photons perfectly at a specific frequency. For a one-dimensional coupled-resonator waveguide, we propose to extend the perfect-reflection region from a specific frequency point to a wide band by placing many atoms individually in the resonators in a finite coordinate region of the waveguide. Such a doped resonator array promises to control the propagation of a practical photon wave packet with a certain momentum distribution instead of a single photon, which is ideally represented by a plane wave with a specific momentum. The studies based on the discrete-coordinate scattering theory indicate that such a hybrid structure with finite atoms indeed provides a near-perfect reflection for a single photon in a wide band. We also calculated the photon group velocity distribution, which shows that the perfect-reflection wide band exactly corresponds to the stopping light region.

DOI: 10.1103/PhysRevA.83.013825 PACS number(s): 42.50.Ex, 03.65.Nk, 85.25.−j

I. INTRODUCTION

Quantum manipulation in all-optical fashions [1–4] is very crucial to the future development of high technology concerning optical communication [1,5–10], the quantum information process [1,5,7,11,12], and the next-generation quantum devices, e.g., single-photon transistors [5,11,13], quantum switches [1,6–10,13–15], and photon storages [2–4,16,17].

The core physics behind all-optical quantum manipulation is to explore the single-photon scattering and propagation in the confined structure of the sizes comparable to the wavelength of the photon. The investigations about the single-photon propagation in one dimension involve some new phenomena, such as the perfect reflection of the single photon by atomic mirror [1,6,7,14,18], slowing light processes [2,3,16,17,19] in hybrid coupled-resonator waveguides, and other related issues [4–6,9,20]. The hybrid structures concerned could be implemented physically with linear defect cavities in photonic crystals [21] with doped quantum dots, or superconducting transmission line resonators [8,10,15] coupled to a superconducting qubit [5,22–25]. These physical systems with artificial band structures coupled to a two-level system enable us to control the transport of a single photon. By tuning the structure parameters of the hybrid system, the two-level system acts as a quantum switch, making the transporting single photon reflect perfectly, or transmit totally. In this sense, the two-level system can behave as an ideal mirror [1,6,7,14,18].

It has been shown that a single-photon transistor using nanoscale surface plasmons [1], coupled with a three-level atom in electromagnetically induced transparency (EIT) setup [2–4,16,17], exhibits controllable behavior in the transmission spectra. We have re-examined the coherent transport of a single photon in a coupled-resonator array coupled to a controllable two-level system [7]. Being different from the linear dispersion relation in the setups by Chang *et al.* [1,6], the cosine-type dispersion [7] will result in two bound states in the hybrid system. The total reflection by the two-level system, which behaves as an ideal mirror, has been found to be associated with the Fano-Feshbach and Breit-Wigner line shapes [26] around the resonance in the reflection spectrum. However, in all of these works [1,6,7], we emphasize that the perfect reflection exists only at a specific frequency point. It brings physical difficulties in practical applications, such as the efficiency to control an optical pulse, which actually is a superposition of the plane waves with different frequencies where the off-resonant components could deviate dramatically from the perfect-reflection point.

In this paper, we propose an experimentally accessible setup based on the coupled-resonator array with a doped-atoms hybrid system, which is expected to realize perfect reflection with a wide spectrum, and thus can perfectly reflect an optical pulse, namely, a single-photon wave packet. Here, we use a "thick" atomic mirror that is made of an array of two-level atoms individually doped in some cavities arranged in a coordinate region of the one-dimensional coupled-cavity waveguide. The physical mechanism is intuitive: When a photon a little far from resonance reaches one cavity coupled to the doped atom, it is reflected by the atom partly, and then the left part passing through the next atom experiences the same process. This process is repeated many times, which may achieve the perfect reflection with a wide spectrum as long as the interference enhancement could be suppressed by some mechanism. The emergence of a wide-band spectrum is also shown schematically in Fig. 1, where the perfect-reflection region is from a specific incident-energy point (for a single atom) to a wide band (for more than one atom).

In detail, we will study the wide-band scattering phenomena for our proposed atomic mirror by using the discrete-coordinate scattering approach [7,14]. With the second-order processes for the atom absorbing a photon and then radiating back inside the cavity, the basic role of the doped atoms is to provide an effective potential such as a local resonant Dirac comb [27], which leads to the stopping and slowing light phenomena [2,3,16,17,19]. By detuning the coupling strength of the atom coupled to the single-cavity mode, we can feasibly

*gongzr@itp.ac.cn
†suncp@itp.ac.cn

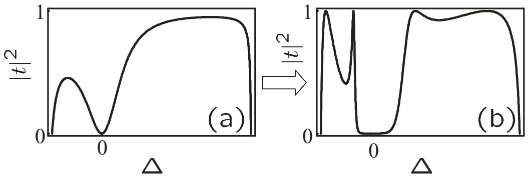

FIG. 1. Schematic diagram for the emergence of the wide band for perfect reflection. Here, Δ is the detuning for the incident photon's energy, and $|t|^2$ is the transmission coefficient. It is shown that for single atom [for (a)], the perfect reflection region is only a specific point; while when the atom number N_a is 3 [for (b)], the region is extended to a wide band.

control the width of the perfect-reflection band. It is noticed that this wide-band spectrum phenomena have been implied in some works [14,20,28].

The paper is organized as follows. In Sec. II, we propose our model and solve it with the discrete-coordinate scattering theory. In Sec. III, we study the microscopic physical mechanism, and then acquire the slowing light phenomenon in Sec. IV. In Sec. V, we study the influence of the imperfections in experiments on the perfect-reflection wide band. We give a summary in Sec. VI.

II. WIDE-BAND ATOMIC MIRROR FOR A SINGLE PHOTON IN ONE DIMENSION

Our hybrid system is shown in Fig. 2, where the N_a two-level atoms are individually embedded in a one-dimensional coupled-resonator waveguide (CRW) [29]. The atoms play an essential role in controlling the propagation of a single photon. The Hamiltonian $H = H_c + H_I$ of this hybrid system consists of two parts, the CRW part described by a tight-binding boson model

$$H_c = \omega \sum_{j=-N}^{N} a_j^\dagger a_j + V \sum_{j=-N}^{N} (a_j^\dagger a_{j+1} + a_{j+1}^\dagger a_j), \tag{1}$$

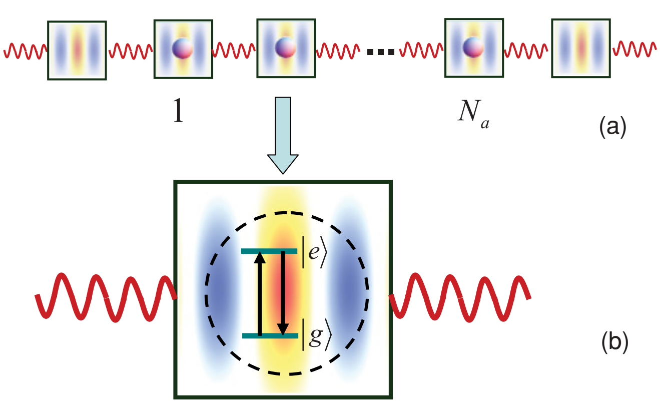

FIG. 2. (Color online) Schematic setup of the wide-band atomic-mirror model. It is constituted by a coupled-resonator waveguide and an array of two-level atoms from 1 to N_a as shown in (a). The coupling between the cavity field and the two-level atom is shown in detail in (b), which is described by the Jaynes-Cumming model. The existence of the N_a atoms can extend the perfect-reflection region to a wide band.

and the part of two-level atoms interacting with the cavity fields

$$H_I = \frac{\Omega}{2} \sum_{j=1}^{N_a} (\sigma_j^z + 1) + g \sum_{j=1}^{N_a} (a_j \sigma_j^+ + a_j^\dagger \sigma_j^-). \tag{2}$$

Here, a_j is the annihilation operator of the jth single-mode cavity with frequency ω, and V is the hopping constant between the nearest-neighbor cavities for the photon. We assume that all the two-level atoms and the cavity fields have the same energy level spacing Ω and frequency ω, respectively. The coupling between each atom and the corresponding cavity field is described by the Jaynes-Cummings model [30] with homogeneous coupling constant g. In Eq. (2), the Pauli spin matrices $\sigma_j^z \equiv |e\rangle_{jj}\langle e| - |g\rangle_{jj}\langle g|$ depict the atomic energy of the jth atom with the ground state $|g\rangle_j$ and exited state $|e\rangle_j$, and $\sigma_j^+ \equiv (\sigma_j^-)^\dagger = |e\rangle_{jj}\langle g|$.

We note that the dispersion relation in the tight-binding boson model in Eq. (1) is of the cosine type, which results in bound states in the hybrid system. Actually, this tight-binding model is quite appropriate for simplifying the physical problem and has inspired extensive interest and lots of attention, both theoretically and experimentally [7,8,21,31–34]. In our previous work [7], we discovered that the electromagnetic field confined in this coupled-resonator waveguide can be well controlled by a single two-level system.

To analyze the transport features of a single photon, we apply the discrete-coordinate scattering approach [7,14] by assuming that the eigenstate of H with eigenenergy E for the incident photon in a single excitation subspace as

$$|\Psi(E)\rangle = \sum_{j=-N}^{N} u_j^g |j\rangle \otimes |G\rangle + |0\rangle \otimes \sum_{j=1}^{N_a} u_j^e |e\rangle_j \otimes |G_j'\rangle, \tag{3}$$

where $|0\rangle$ represents the vacuum of the cavity fields, $|j\rangle = a_j^\dagger |0\rangle$, and

$$|G\rangle = \prod_{j=1}^{N_a} |g\rangle_j, \quad |G_j'\rangle = \prod_{l=1, l\neq j}^{N_a} |g\rangle_l. \tag{4}$$

Here, u_j^g and u_j^e are the amplitudes of the single photon and the atomic population in the jth cavity, respectively. The first term on the right-hand side of Eq. (3) depicts the single photon propagating along the waveguide, while the second term represents that the photon is "captured" by an atom. It follows from the Schrödinger equation $H|\Psi(E)\rangle = E|\Psi(E)\rangle$ that the scattering equations for a single photon with discrete-coordinate representation read as

$$\omega u_j^g + V\left(u_{j+1}^g + u_{j-1}^g\right) + W(E) u_j^g = E u_j^g. \tag{5}$$

Here, the effective potential

$$W(E) = w(E) \sum_{l=1}^{N_a} \delta_{jl} \tag{6}$$

is like a local resonant Dirac comb [27] with strength $w(E) = g^2/(E-\Omega)$. The equations related to the atomic population are

$$\Omega u_j^e + g u_j^g = E u_j^e. \tag{7}$$

We indicate here that u_j^g and u_j^e in Eq. (3) depend on the energy E of the incident photon, and the interaction between the cavity fields and the atoms provides the potential $W(E)$ to affect the propagation of the single photon. Equation (5) shows that, due to the array of atoms, the incident single photon acquires an additional potential described by the local resonant Dirac comb, and the strength of this potential, i.e., $w(E)$, depends on the incident photon's energy E. On resonance, i.e., $E = \Omega$, the strength $w(E)$ of the effective potential is infinite, which definitely leads to the perfect reflection of the incident photon. This result is consistent with that in the previous work [7]. For the scattering in one dimension, in which the eigenfunction only possesses the reflection and transmission waves, the solutions to Eq. (5) for $j \neq 1, 2, \ldots, N_a$ are

$$u_j^g = \begin{cases} e^{ikj} + re^{-ikj}, & j < 1 \\ te^{ikj}, & j > N_a \end{cases}, \tag{8}$$

where r and t are reflection and transmission amplitudes, respectively. To consider elastic scattering, we can use the eigenvalue of the scattered photon

$$E(k) = \omega + 2V\cos k \tag{9}$$

with the cosine-type dispersion for the incident photon with momentum k.

The solutions in the region where the cavity fields interact with the atoms are

$$u_j^g = r'e^{-ik'j} + t'e^{ik'j}, \tag{10}$$

for $j = 1,2,\ldots,N_a$, where k' is the solution of the transcendental equation

$$2V\cos k' = 2V\cos k - w(E), \tag{11}$$

which exhibits the conservation of energy. In Eqs. (8) and (10), r and t, together with r' and t', are determined in the following by four boundary conditions, i.e., the scattering Eq. (5) in four points $j = 0, 1, N_a$, and $N_a + 1$. The transmission coefficient $|t|^2$ is then obtained as

$$|t|^2 = \left| \frac{4V^2 \sin k \sin k'}{A(E)^2 e^{ik'(N_a-1)} - B(E)^2 e^{-ik'(N_a-1)}} \right|^2, \tag{12}$$

corresponding to the reflection coefficients $|r|^2 = 1 - |t|^2$, where

$$A(E) = Ve^{-ik'} - Ve^{-ik} + w(E) \tag{13}$$

and

$$B(E) = Ve^{ik'} - Ve^{-ik} + w(E) \tag{14}$$

are independent of N_a.

Furthermore, it follows from Eq. (11) that, when

$$\left| \cos k - \frac{w(E)}{2V} \right| \geqslant 1, \tag{15}$$

k' is complex or $k' = n\pi$ (n is an integer), which exhibits the photon's probability of decaying in the interaction region.

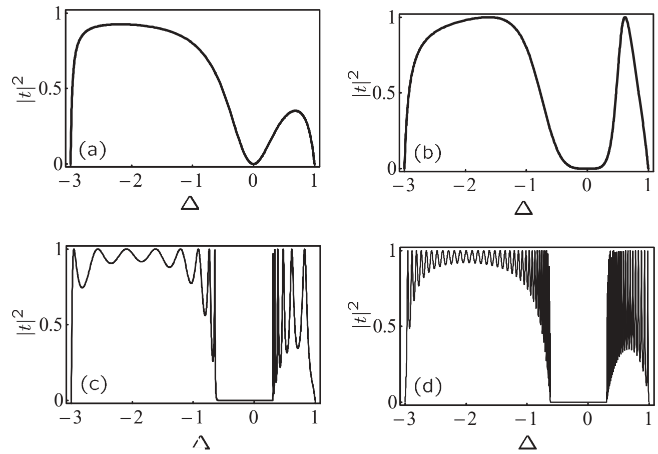

FIG. 3. The transmission spectrum $|t|^2$ as a function of the detuning Δ for different atom numbers N_a, where (a) $N_a = 1$, (b) $N_a = 2$, (c) $N_a = 10$, and (d) $N_a = 50$. The wide band of perfect reflection ($|t|^2 = 0$) emerges gradually as the atom number N_a increases. When doping only a few atoms (such as $N_a = 10$), the near-perfect reflection band can fit the practical application. When the atom number N_a tends to infinity, the region of the wide band reaches its maximum.

When $k' = n\pi$, Eq. (12) gives $|t|^2 = 0$. When k' is complex, it is shown in Eq. (12) that $|t|^2 \to 0$ when $N_a \to +\infty$. In this case, the array of atoms behaves as a mirror that reflects the light perfectly.

The transmission spectra $|t|^2$ in Eq. (12) versus the detuning $\Delta = E(k) - \Omega$ for different atom numbers N_a are shown in Figs. 3(a)–3(d). The parameters in these figures are chosen as $\omega = 5g$, $\Omega = 6g$, and $V = -g$. These figures show that as N_a increases, the width of the perfect-reflection band near the resonance $\Delta = 0$ increases correspondingly and at last reaches its maximum value with large N_a. In contrast to the single-atom-mirror case with only one specific reflection frequency, such multiatom mirrors can be used to manipulate the propagation of a practical wave packet, the distribution in momentum space of which is restricted in the wide-band reflection region.

III. FREQUENT REFLECTIONS INDUCED SPECTRUM BROADENING

We have obtained the wide band for perfect reflection by solving the discrete-coordinate scattering Eq. (5) in Sec. II. In this section, we study the physical mechanism of this wide band and find the rigorous boundaries of the band.

As shown in Ref. [7], for a single atom at the 0th single-mode cavity, the reflection and transmission amplitudes for a single incident photon with momentum k are

$$r_1(k) = \frac{g^2}{-2iV(E-\Omega)\sin k - g^2} \tag{16}$$

and

$$t_1(k) = \frac{2iV(E-\Omega)\sin k}{2iV(E-\Omega)\sin k + g^2}, \tag{17}$$

respectively. The corresponding normalized eigenstate is

$$|\Omega(k)\rangle = \frac{1}{\sqrt{2\pi}} \sum_{j=-N}^{N} \xi_j^g a_j^\dagger |0\rangle |g\rangle_0 + \xi^e |0\rangle |e\rangle_0, \tag{18}$$

where

$$\xi_j^g(k) = \begin{cases} e^{ikj} + r_1(k)e^{-ikj}, & j < 0 \\ t_1(k)e^{ikj}, & j \geqslant 0 \end{cases} \quad \text{for } k > 0 \tag{19}$$

and

$$\xi_j^g(k) = \begin{cases} e^{ikj} + r_1(-k)e^{-ikj}, & j > 0 \\ t_1(-k)e^{ikj}, & j \leqslant 0 \end{cases} \quad \text{for } k < 0. \tag{20}$$

These reflection and transmission amplitudes are consistent in magnitudes with the results that we have acquired in Eq. (12) when $N_a = 1$.

An element S_{kp} of the S matrix describing the probability amplitude of an outgoing photon with momentum k when the incident photon momentum is p in this single-atom system is

$$S_{kp} = \delta_{kp} - i2\pi\delta_{E(k)E(p)} \langle k|V_{int}|\Omega(p)\rangle, \tag{21}$$

where

$$|k\rangle = \frac{1}{\sqrt{2\pi}} \sum_{j=-N}^{N} e^{ikj} a_j^\dagger |0\rangle |g\rangle_0 \tag{22}$$

is the outgoing state with momentum k, and

$$V_{\text{int}} = g(a_0\sigma_0^+ + a_0^\dagger \sigma_0^-) \tag{23}$$

is the photon-atom coupling. Following these definitions, the S-matrix element reads as

$$S_{kp} = \begin{cases} t_1(p)\delta_{kp} + r_1(p)\delta_{-k,p}, & p > 0 \\ t_1(-p)\delta_{kp} + r_1(-p)\delta_{-k,p}, & p < 0 \end{cases}. \tag{24}$$

Neglecting the interference between the reflection and transmission waves in the interaction region, the scattering matrix element $S'_{k,k}$ corresponding to the transmission amplitude for N_a atoms is written approximately as

$$S'_{k,k} \approx (S_{k,k})^{N_a} = t_1^{N_a}. \tag{25}$$

To investigate this approximation condition, we expand $|t|^2$ shown in Eq. (12) around the point $\Delta = 0$ as

$$|t|^2 \approx \left(\frac{V}{g^2}\right)^{2N_a} \frac{4V^2 - \delta^2}{V^2} \Delta^{2N_a} + o(\Delta^{2N_a}), \tag{26}$$

where we have made an approximation that $|2V\cos k| \ll |w(E)|$. With this expansion (26), we expand $|t_1|^{2N_a}$ approximately as

$$|t_1|^{2N_a} \approx \left(\frac{4V^2 - \delta^2}{g^4}\right)^{N_a} \Delta^{2N_a} + o(\Delta^{2N_a}). \tag{27}$$

It is shown in Eqs. (26) and (27) that, in the region near the resonance, both $|t|^2$ and $|t_1|^{2N_a}$ tend to zero with the power-law function Δ^{2N_a}. Thus, it indicates that the emergence of the wide band near the resonance is due to the incoherent reflection by the array of atoms.

This approximate transmission coefficient is plotted in Fig. 4 in contrast with the rigorous solution shown in Fig. 3(c).

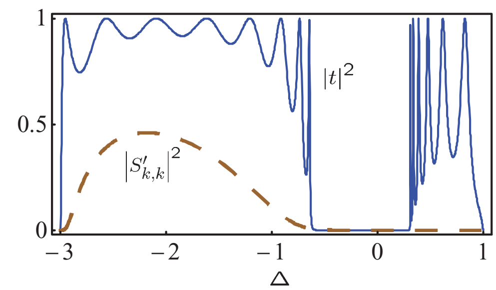

FIG. 4. (Color online) The transmission coefficient $|S'_{k,k}|^2 \equiv |t_1|^{2N_a}$ (brown dashed line) with respect to the detuning Δ in the approximation shown in Eq. (25) with $N_a = 10$. The other parameters are the same as those in Fig. 3. For comparison, the exact result $|t|^2$ (blue solid line) is plotted in this figure. It is shown that perfect-reflection wide bands appear in both $|S'_{k,k}|^2$ and $|t|^2$, which are due to the reflection of light by multiatoms. The widths of these two bands are different, as we do not take into account the interference of the reflection and transmission waves between different atoms in $|S'_{k,k}|^2$. Furthermore, the interference effect leads to the resonant transmission peaks in the transmission spectrum.

Apparently, the wide-band perfect-reflection phenomenon also appears in the approximate transmission coefficient. It demonstrates that the appearance of the wide band is due to the reflection of light by the array of atoms. In other words, when the light reaches the first cavity coupled to a doped atom, the incident photon only has the probability $|t_1|^2$ to pass through the atom. Then, the second atom repeats this reflection process when the light passes through it and the transmission coefficient becomes $|t_1|^4$. This process is repeated by N_a atoms when the light passes through and eventually leads to the transmission coefficient as $|t_1|^{2N_a}$. In this discussion, we do not take into account the interference effect at all, as the construction of the wide band is only dominated by individual reflection processes. Actually, when considering the interference of reflection and transmission waves between atoms, the region forbidding light propagation varies greatly. The interference effect also leads to the resonate transmission peaks in the transmission spectrum (see the peaks in Fig. 4).

The width of the perfect-reflection band is determined by taking the imaginary part of the momentum k' as nonzero or $k' = n\pi$. We notice that, in Eq. (11), when

$$\cos k' = \frac{E - \omega - w(E)}{2V} \geqslant 1, \tag{28}$$

the wave vector k' is complex:

$$k'_+ = 2n_+\pi + i\alpha_+. \tag{29}$$

On the other hand, when

$$\cos k' = \frac{E - \omega - w(E)}{2V} \leqslant -1, \tag{30}$$

k' takes the form

$$k'_- = (2n_- + 1)\pi + i\alpha_-. \tag{31}$$

Here, $n_\pm$ are integers and $\alpha_\pm$ are real. If k' has the form shown in Eqs. (29) or (31), the denominator in Eq. (12) tends to infinity while $N_a$is sufficiently large, which results in the vanishing transmission coefficient.

It follows from Eqs. (28) and (30) that the range for the incident photon energy E is

$$\max\{E_-, E_{\min}\} \leqslant E \leqslant \min\{\Omega, E_{\max}\} \tag{32}$$

or

$$\max\{\Omega, E_{\min}\} \leqslant E \leqslant \min\{E_+, E_{\max}\}, \tag{33}$$

where

$$E_\pm = \frac{1}{2}(\omega+\Omega) \mp |V| \pm \sqrt{\left(\frac{\delta}{2} \mp |V|\right)^2 + g^2}, \tag{34}$$

$$E_{\max} = \omega + 2|V|, \quad E_{\min} = \omega - 2|V|, \tag{35}$$

and

$$\delta = \omega - \Omega. \tag{36}$$

When E is in this range determined by Eqs. (32) and (33), with many atoms, the photon is reflected perfectly.

When $g = 0$, the wide-band width $L = 0$, which corresponds to our common sense that the photon propagates freely along the CRW without coupling to atoms. With the set of parameters in Fig. 3, the width L is $E_+ - E_-$, with the resonant point $\Delta = 0$ in the wide band. However, note that, with some other parameters, the point $\Delta = 0$ does not locate inside the wide band. Additionally, when the parameters satisfy one of the following conditions, the band width is $4|V|$: (i) $E_- \leqslant E_{\min} \leqslant \Omega \leqslant E_{\max} \leqslant E_+$; (ii) $E_{\min} \geqslant \Omega$ and $E_+ \geqslant E_{\max}$; and (iii) $E_{\min} \leqslant \Omega$ and $E_- < E_{\min}$. Namely, by tuning the parameters in this region, the light can be reflected perfectly in the whole region of the energy of the incident photon. With the other parameters, which are the same as those in Fig. 3, we plot the wide-band width L with respect to the parameters V, g, Ω, and ω, respectively, in Figs. 5(a)–5(d). It is shown in Fig. 5(a) that when $V = 0$, which means that the photon can not hop in the CRW, $L = 0$. As $|V|$ increases, L increases until $|V|$ reaches some critical point. L then decreases when $|V|$ increases, since in this range, the larger the hopping strength $|V|$, the weaker the photon-atom coupling becomes as a perturbation. In Fig. 5(b), L is a monotonic increasing function of the atom-photon coupling strength $|g|$, and L reaches the maximum $4|V|$. Namely, the stronger coupling leads to a wider perfect-reflection band. Figures 5(c) and 5(d) show that, when Ω or ω is very large, i.e., the difference between the incident photon's energy $E(k)$ and the two-level atom's energy level spacing Ω is very large, L tends to zero. The reason leading to this behavior is similar to that in the rotating-wave approximation [30], i.e., the large energy difference makes the interaction negligible with large time scale.

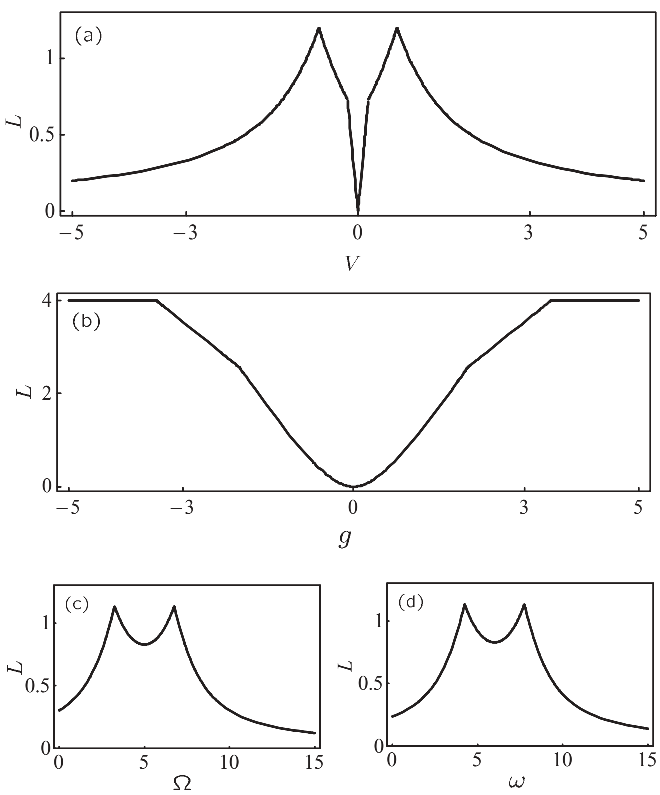

FIG. 5. The width L for the perfect-reflection band as a function of the parameters (a) V, (b) g, (c) Ω, and (d) ω, with the other parameters the same as those in Fig. 3. In (a), L first increases and then decreases with the increment of $|V|$. In (b), the width L increases as the atom-photon coupling strength $|g|$ increases, and L reaches its maximum $4|V|$. In (c) and (d), in the region where the difference between the incident photon's energy and the atom's energy level spacing is very large, the width L tends to zero.

The width of the perfect-reflection band is obtained with large N_a. We now discuss how large N_a is to ensure that our results are reliable. With the parameters in Fig. 3, the boundaries $\Delta_\pm$ of the wide band are acquired using Eqs. (32) and (33) as

$$\Delta_- \approx -0.618g \quad \text{and} \quad \Delta_+ \approx 0.302g. \tag{37}$$

We plot the transmission coefficients $|t|^2$ in these two boundaries with respect to N_a in Fig. 6. When $N_a \geqslant 20$, the transmission coefficients in both boundaries vanish approximately. As a result, the width we obtained of perfect reflection does not require $N_a \to \infty$ in practice. In fact, with this set

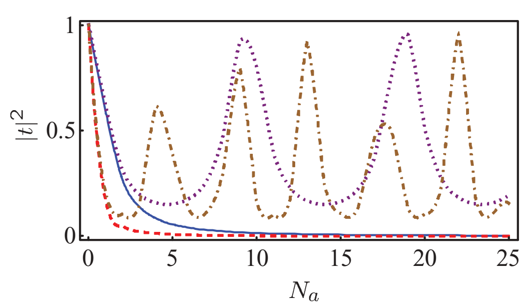

FIG. 6. (Color online) The transmission coefficients $|t|^2$ in two boundaries $\Delta_\pm$ with respect to N_a, where the blue dotted line represents $|t|^2$ in the left boundary, while the red dashed line represents $|t|^2$ in the right boundary. When $N_a \geqslant 20$, the transmission coefficients in both boundaries vanish approximately. With this set of parameters, 20 is large enough for N_a to ensure the reliability for the width of the perfect-reflection band that we obtained. For comparison, the transmission coefficients with the energy beyond the wide band are plotted (the purple dotted line for $\Delta = -0.65$ and the brown dot-dashed line for $\Delta = 0.35$). The transmission coefficients $|t|^2$ do not tend to zero as the atom number N_a increases unless the energy is in the wide band.

of parameters in Fig. 6, $N_a = 20$ is large enough to build the wide band for perfect reflection. For comparison, we also plot $|t|^2$ versus N_a with the energies beyond the wide band, which show that $|t|^2$ does not tend to zero with the increment of N_a, even though the energy is very close to that at the boundaries $\Delta_\pm$.

IV. SLOW LIGHT RESONANT ABSORPTION

We have shown the wide-band reflection by a multiatomic mirror. We now consider the slowing and stopping light phenomena in the interaction region with an array of atoms, which actually has a close relation to the emergence of the wide band [34].

We revisit the Hamiltonian in the interaction region

$$H_{\text{int}} = \sum_{j=1}^{N_a} \omega a_j^\dagger a_j + V \sum_{j=1}^{N_a-1} (a_j^\dagger a_{j+1} + a_{j+1}^\dagger a_j) + \sum_{j=1}^{N_a} \left[\frac{\Omega}{2}(\sigma_j^z + 1) + g(a_j \sigma_j^+ + a_j^\dagger \sigma_j^-) \right]. \quad (38)$$

The corresponding eigenstates for Eq. (38) are

$$|\Psi_{\text{int}}\rangle = \sum_{j=1}^{N_a} v_j^g |j\rangle \otimes |G\rangle + |0\rangle \sum_{j=1}^{N_a} v_j^e |e\rangle_j \otimes |G'_j\rangle, \quad (39)$$

with the eigenvalue E that is determined by the set of equations

$$\omega v_j^g + V\left(v_{j+1}^g + v_{j-1}^g\right) + w(E) v_j^g = E v_j^g, \quad j = 2,\ldots,N_a - 1, \quad (40)$$

$$\omega v_1^g + V v_1^g + w(E) v_1^g = E v_1^g, \quad (41)$$

$$\omega v_{N_a}^g + V v_{N_a-1}^g + w(E) v_{N_a}^g = E v_{N_a}^g, \quad (42)$$

and

$$\Omega v_j^e + g v_j^g = E v_j^e. \quad (43)$$

We note that the difference between Eqs. (40)–(42) and Eq. (5) is the different boundary condition. The solutions to the set of Eqs. (40)–(42) are

$$v_j^g = A \sin\, pj, \quad (44)$$

with normalization constant A, and the eigenvalues satisfy

$$E_{\text{int}} = \omega + \frac{g^2}{E_{\text{int}} - \Omega} + 2V \cos p, \quad (45)$$

where p is determined by the boundary conditions (41) and (42) as

$$p = \frac{n\pi}{N_a + 1}, \quad n = 1,\ldots,N_a. \quad (46)$$

Consequently,

$$E_{\text{int}}^{\pm}(p) = \tfrac{1}{2}\left(\delta_p \pm \sqrt{\delta_p^2 + 4g^2}\right) + \Omega, \quad (47)$$

where $\delta_p = \delta + 2V\cos p$.

It is shown in Eq. (47) that there are two energy bands for the interaction region, which are labeled by E_{int}^+ and E_{int}^-. The two bands are shown schematically in Fig. 7(a). When N_a tends to infinity, the energy at bottom of the upper band E_{int}^+ is E_+, and at top of the lower band E_{int}^- the energy is E_-, with the band gap $L = E_+ - E_-$ as shown in Eqs. (32) and (33). The band gap for the interaction region contains the wide band for perfect reflection of a single photon. Namely, when the incident photon energy is in the band gap, it is impossible for the photon to go through the interaction region. With large N_a, we plot $E_{\text{int}}^{\pm}(p)$ with respect to p in Fig. 7(b). Here, the parameters are the same as those in Fig. 3. We note that the incident electron energy corresponding to the resonant peaks in the transmission spectrum is not in agreement with the eigenenergies that we obtained in Eq. (47) in the interaction region.

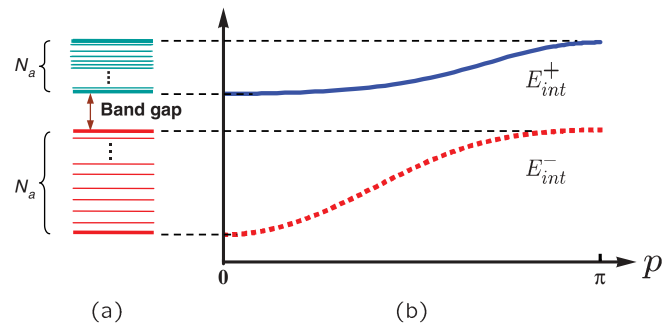

FIG. 7. (Color online) Schematic configuration for the two energy bands $E_{\text{int}}^{\pm}$ [for (a)]. Here, each band has N_a energy levels. When N_a energy levels tends to infinity, $E_{\text{int}}^{\pm}(p)$ with respect to p is shown in (b), with the band gap $E^+ - E^-$.

The group velocity v_g of light propagating in the interaction region is defined as

$$v_g^{\pm}(p) = \partial_p E_{\text{int}}^{\pm}(p). \quad (48)$$

Since the momentum k' in the interaction region depends on the energy E of the incident photon, the group velocity v_g is also dependent on E. However, when E is in the band gap, k' is complex and $v_g(\Delta)$ is also complex. This complex $v_g(\Delta)$ depicts the decay in the light propagating in the interaction region. In this sense, when N_a is large, this group velocity is zero. It demonstrates that the stopping light phenomenon is due to the atomic mirror. The group velocities in the two bands are plotted in Fig. 8 with the same parameters as those in Fig. 3. For comparison, we also plot the group velocity $v_g = -2V \sin k$ in the CRW without doping atoms. When $\Delta < 0$, the photon propagates in the lower band, while when $\Delta > 0$, the photon propagates in the upper band. Figure 8 shows the slowing and stopping light phenomena in the interaction region, and the width of Δ in the light stopping region corresponds exactly to the width of the perfect-reflection band shown in Fig. 3(d).

We note that these results are based on the assumption that N_a is large, or even infinite. However, in practical applications, N_a is finite and maybe not very large, so the reflection in the whole of the band would not be so perfect. We investigate the influence of N_a on the perfect-reflection wide band and show that, with some parameters, $N_a = 20$ is large enough to ensure the the reliability of our results.

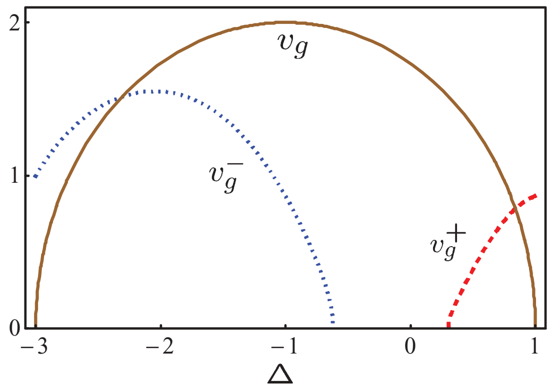

FIG. 8. (Color online) The light group velocity v_g^- (dotted blue line), v_g^+ (dashed red line), and v_g (solid brown line) for lower band E^-, upper band E^+, and free tight-binding model $E(k)$ vs the detuning Δ. The region where $v_g^\pm = 0$ depicting the stopping light phenomenon exactly corresponds to the wide band for perfect reflection.

V. INFLUENCE OF IMPERFECTIONS IN EXPERIMENTAL IMPLEMENTS

In experiments, the atomic decay, the intrinsic loss of each coupled resonator, and the disorder [21,35,36] in the CRW are inevitable. In this section, we investigate how these imperfections influence the frequency wide band for the perfect reflection that we have studied. First, we consider the disorder problem without atomic decay and losses of coupled resonators.

In principle, the whole CRW scale can be infinite, thus we only consider a segment of disordered resonators. Moreover, we assume that the disordered region happens to the atom-cavity interaction region, which means that the hopping constant V_j for $i,\ j \in [1, N_a - 1]$, and the on-site frequency ω_j for $j \in [1, N_a]$ becomes position dependent. Under these assumptions, the total Hamiltonian

$$H_{\text{imp}} = H_L + H_{\text{int}}^D \tag{49}$$

is divided into two parts: as the lead part,

$$H_L = \omega \left(\sum_{j=-N}^{0} + \sum_{j=N_a+1}^{N} \right) a_j^\dagger a_j \tag{50}$$

$$+ V \left(\sum_{j=-N}^{0} + \sum_{j=N_a}^{N} \right) (a_j^\dagger a_{j+1} + a_{j+1}^\dagger a_j), \tag{51}$$

and the disordered part in the atom-cavity interaction region is

$$\begin{aligned} H_{\text{int}}^D &= \sum_{j=1}^{N_a} \omega_j a_j^\dagger a_j + \sum_{j=1}^{N_a-1} V_j (a_j^\dagger a_{j+1} + a_{j+1}^\dagger a_j) \\ &+ \sum_{j=1}^{N_a} \left[\frac{\Omega}{2} (\sigma_j^z + 1) + g (a_j \sigma_j^+ + a_j^\dagger \sigma_j^-) \right]. \end{aligned} \tag{52}$$

The eigenstate of H_{imp} with eigenenergy $E = \omega + 2V \cos k$ for the incident photon with momentum k in the single excitation subspace has a form similar to that in Eq. (3):

$$|\Phi(E)\rangle = \left(\sum_{j=-N}^{0} + \sum_{j=N_a+1}^{N} \right) \phi_j |j\rangle \otimes |G\rangle + |\Phi_D(E)\rangle, \tag{53}$$

where the amplitudes in the lead part's wave function can still be assumed to describe the reflection and transmission as

$$\phi_j = \begin{cases} e^{ikj} + r_D e^{-ikj}, & j < 1 \\ t_D e^{ikj}, & j > N_a \end{cases}, \tag{54}$$

and

$$|\Phi_D(E)\rangle = \sum_{j=1}^{N_a} \phi_j^g |j\rangle \otimes |G\rangle + |0\rangle \otimes \phi_j^e |e\rangle_j \otimes |G_j'\rangle \tag{55}$$

is the wave function in the atom-cavity interaction region. Here, r_L and t_L are the reflection and transmission amplitudes, respectively. Resulting from the boundary conditions at points $j = 1$ and $j = N_a$, respectively, these amplitudes satisfy

$$r_D = e^{ik} (\phi_1^g - e^{ik}), \tag{56}$$

$$t_D = e^{-ikN_a} \phi_{N_a}^g. \tag{57}$$

By solving the Schrödinger equation $H_{\text{imp}} |\Phi(E)\rangle = E |\Phi(E)\rangle$, we straightforwardly obtain the equation for $|\Phi_D(E)\rangle$ as

$$|\Phi_D(E)\rangle = V(e^{2ik} - 1) w |1\rangle \otimes |G\rangle, \tag{58}$$

where

$$w = \frac{1}{H^D + V e^{ik} (a_1^\dagger a_1 + a_{N_a}^\dagger a_{N_a}) - E} \tag{59}$$

is the inverse of the Hamiltonian matrix together with the contributions of the lead part.

The amplitudes ϕ_1^g and $\phi_{N_a}^g$ are completely determined by the $2N_a \times 2N_a$ matrix w. Since the disorder exists in the atom-cavity interaction region, the inhomogeneity of the hopping constants $\{V_j\}$ and the on-site frequencies $\{\omega_j\}$ are expected to destroy the coherence of the incident photon and, hence, enhance the reflection. For a particular realization of disorder, i.e., for given sets $\{\omega_j\}$ and $\{V_j\}$, which are generated randomly in the ranges $[\omega - 0.2\omega,\ \omega + 0.2\omega]$ and $[V - 0.2V, V + 0.2V]$, respectively, we plot the transmission coefficient $|t_D|^2$ versus the detuning $\Delta = E(k) - \Omega$ in Fig. 9(a). The other parameters are the same as those in Fig. 3(c). Figure 9(a) shows that the wide band is almost unaffected, while outside the wide band the transmission coefficient is changed dramatically. We assume that the disorder in the atom-cavity interaction region has the Gaussian distribution of both $\{\omega_j\}$ and $\{V_j\}$ as

$$P(x) = \frac{\exp[(x - x_0)^2 / 2\sigma^2]}{2\pi\sigma}, \tag{60}$$

where $P(x)$ is the probability for a given value x, $x = \omega_j$, V_j, x_0 is the averaged value, and σ is the variance. We plot the averaged transmission coefficient $|t_D|^2$ versus Δ in Figs. 9(b)–9(d). Here, for the sets $\{\omega_j\}$ and $\{V_j\}$, $x_0 = \omega$ and V, and the variances are 0.01ω and $0.01|V|$ for Fig. 9(b), 0.05ω and $0.05|V|$ for Fig. 9(c), and 0.1ω and $0.1|V|$ for Fig. 9(d). It is shown that Fig. 9(b) is quite similar to Fig. 3(c),

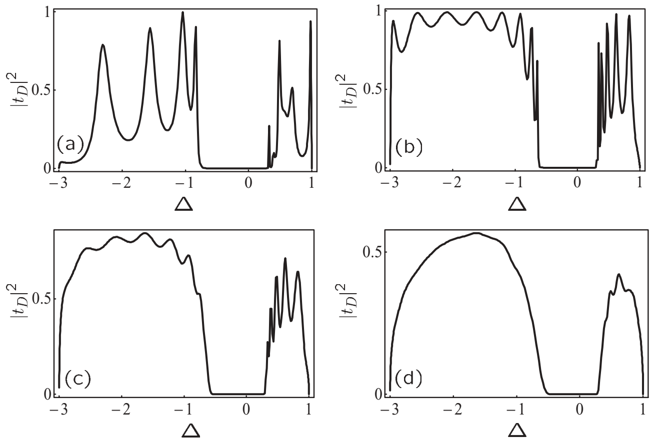

FIG. 9. The transmission coefficient $|t_D|^2$ as a function of the detuning Δ when the frequencies $\{\omega_j\}$ of the cavities and the coupling strength $\{V_{ij}\}$ between the nearest two cavities are different from site to site due to disorder. (a) For given sets $\{\omega_j\}$ and $\{V_{ij}\}$, the wide band for perfect reflection is almost unchanged, while $|t_D|^2$ changes dramatically outside of the wide band. (b)–(d) show the averaged results of the $\{\omega_j\}$ and $\{V_{ij}\}$ when the distributions of $\{\omega_j\}$ and $\{V_{ij}\}$ are Gaussian with the same mean values ω and V, but different variances. When the variances of $\{\omega_j\}$ and $\{V_{ij}\}$ are sufficiently small, e.g., 0.01ω and $0.01|V|$ [for (b)], the transmission curve is quite similar to that in Fig. 3(c). When the variances are increased, e.g., to 0.05ω and $0.05|V|$ [for (c)], and 0.1ω and $0.1|V|$ [for (d)], the range of the wide band is shortened; in the other region, the transmission curve is smoothed, with the depressed envelope, which demonstrates the destruction of the coherence of the incident photon due to the existence of the disorder.

both in the perfect- and nonperfect-reflection regions. When the variances of $\{\omega_j\}$ and $\{V_j\}$ increase, the range of the wide band is shortened.

The atomic decay and the loss of resonators also play an essential role in experiments. Usually, such atomic decay and resonator losses mean inelastic scattering, which results from the interaction between the system and a realistic environment described by phonons. For simplicity, we investigate this effect on the perfect-reflection wide band by phenomenologically adding imaginary parts $-i\gamma_a$ and $-i\gamma_c$ to the two-level atom frequency Ω and the coupled-resonator frequency ω, respectively. We note that these losses will can be directly added in the final results [see Eq. (12)] phenomenologically. As a result, without disorders, the transmission coefficient in Eq. (12) becomes

$$|t_L|^2 = \left|\frac{4V^2 \sin\, k \sin k_L'}{C(E_L)^2 e^{ik_L'(N_a-1)} - D(E_L)^2 e^{-ik_L'(N_a-1)}}\right|^2, \quad (61)$$

where

$$C(E_L) = Ve^{-ik_L'} - Ve^{-ik} + w_L(E_L), \quad (62)$$
$$D(E_L) = Ve^{ik_L'} - Ve^{-ik} + w_L(E_L), \quad (63)$$

and k_L' satisfies the equation

$$2V\cos\, k_L' = 2V\cos k - w_L(E). \quad (64)$$

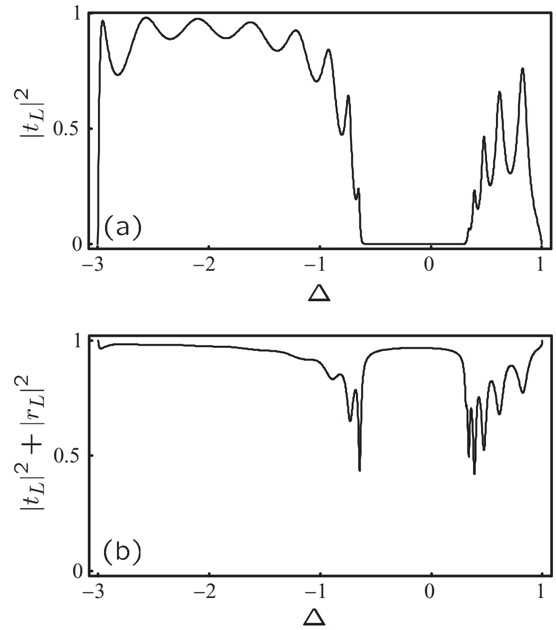

FIG. 10. The transmission coefficients (a) $|t_L|^2$ and (b) $|r_L|^2 + |t_L|^2$ with respect to the detuning Δ in the system environment interacting case. It is shown that the perfect-reflection band still exists, and the photon current is no longer conserved.

Here, $w_L(E_L) = g^2/[E_L - (\Omega - i\gamma_a)]$ and $E_L = \omega - i\gamma_c + 2V\cos k$. The corresponding reflection coefficient is

$$|r_L|^2 = \left|\mathrm{i}2V\sin k\frac{C(E_L) - D(E_L)e^{-i2k_L'(N_a-1)}}{C(E_L)^2 - D(E_L)^2 e^{-i2k_L'(N_a-1)}} - 1\right|^2. \quad (65)$$

With the same parameters in Fig. 3(c), we plot the transmission spectrum $|t_L|^2$ and $|r_L|^2 + |t_L|^2$ in Fig. 10, where $\gamma_a = 0.02g$ and $\gamma_c = 0.01g$. It is shown in Fig. 10(a) that the wide band for perfect reflection also exists in the transmission spectrum, with almost the same boundaries when γ_a/Ω, $\gamma_c/\omega \ll 1$, and $\gamma_a > \gamma_c$ are satisfied, but the envelope of the transmission curve is depressed globally. This phenomenon also appears in Fig. 10(b), which shows that the photon current is not conserved any more, especially near the two boundaries $\Delta_\pm$. However, when the single photon stops in the interaction region, the energy is almost conserved. From this discussion, the wide band for near-perfect reflection is almost not influenced by the imperfections such as disorder, atomic decay, and resonator losses existing in the realistic experiments.

VI. SUMMARY

We have studied the coherent transport of a single photon in a one-dimensional array of coupled resonators individually coupled to two-level atoms. The discrete-coordinate scattering approach shows that a wide-band spectrum appears for a perfect reflection when the number of atoms N_a is large. The physical mechanism for this wide band is considered by the incoherent multireflection for light by N_a atoms, which extends the the perfect reflection line to form a wide band. The slowing and stopping light phenomena also appear due to the interaction with atoms. We also diagonalize exactly the photon-atom interaction Hamiltonian in the interaction region, and obtain two energy bands. It is found that the perfect-reflection wide band is embedded in this band gap. We also consider the effect of imperfections in experimental implements and find that the wide band for near-perfect reflection is not influenced when the parameters describing the imperfections are small.

The model we propose here can be realized by a circuit QED system [5,22–24], where the CRW can by realized by either defect resonators in photonic crystals [21] or coupled superconducting transmission line resonators [8,10,15]. By engineering the photon-atom coupling strengths and other parameters such as the hopping constant and the energy space between the two levels of the atoms, we can control the width and position of the perfect-reflection wide band.

ACKNOWLEDGMENTS

The work was supported by NSFC Grants No. 10474104, No. 60433050, and No. 10704023, and by NFRPC Grants No. 2006CB921205 and No. 2005CB724508.

[1] D. E. Chang, A. S. Sørensen, E. A. Demler, and M. D. Lukin, Nat. Phys. **3**, 807 (2007).
[2] C. P. Sun, Y. Li, and X. F. Liu, Phys. Rev. Lett. **91**, 147903 (2003).
[3] Y. Li and C. P. Sun, Phys. Rev. A **69**, 051802(R) (2004).
[4] Z. R. Gong, H. Ian, L. Zhou, and C. P. Sun, Phys. Rev. A **78**, 053806 (2008).
[5] A. Wallraff, D. I. Schuster, A. Blais, L. Frunzio, R.-S. Huang, J. Majer, S. Kumar, S. M. Girvin, and R. J. Schoelkopf, Nature (London) **431**, 162 (2004).
[6] J. T. Shen and S. Fan, Phys. Rev. Lett. **95**, 213001 (2005).
[7] L. Zhou, Z. R. Gong, Yu-xi Liu, C. P. Sun, and F. Nori, Phys. Rev. Lett. **101**, 100501 (2008).
[8] L. Zhou, Y. B. Gao, Z. Song, and C. P. Sun, Phys. Rev. A **77**, 013831 (2008).
[9] L. Zhou, S. Yang, Yu-xi Liu, C. P. Sun, and F. Nori, Phys. Rev. A **80**, 062109 (2009).
[10] J. Q. Liao, Z. R. Gong, L. Zhou, Yu-xi Liu, C. P. Sun, and F. Nori, Phys. Rev. A **81**, 042304 (2010).
[11] M. Hijlkema, B. Weber, H. P. Specht, S. C. Webster, A. Kuhn, and G. Rempe, Nat. Phys. **3**, 253 (2007).
[12] D. Bouwmeester, A. Ekert, and A. Zeilinger, *The Physics of Quantum Information* (Springer, Berlin, 2000).
[13] M. Orrit, Nat. Phys. **3**, 755 (2007).
[14] L. Zhou, H. Dong, Yu-xi Liu, C. P. Sun, and F. Nori, Phys. Rev. A **78**, 063827 (2008).
[15] J. Q. Liao, J. F. Huang, Yu-xi Liu, L. M. Kuang, and C. P. Sun, Phys. Rev. A **80**, 014301 (2009).
[16] D. L. Zhou, L. Zhou, R. Q. Wang, S. Yi, and C. P. Sun, Phys. Rev. A **76**, 055801 (2007).
[17] L. Zhou, J. Lu, D. L. Zhou, and C. P. Sun, Phys. Rev. A **77**, 023816 (2008).
[18] M. Olshanii, Phys. Rev. Lett. **81**, 938 (1998).
[19] M. Patterson, S. Hughes, S. Combrié, N. V. Q. Tran, A. D. Rossi, R. Gabet, and Y. Jaouën, Phys. Rev. Lett. **102**, 253903 (2009).
[20] T. S. Tsoi and C. K. Law, Phys. Rev. A **78**, 063832 (2008).
[21] A. D. Greentree, C. Tahan, J. H. Cole, and L. C. L. Hollenberg, Nat. Phys. **2**, 856 (2006).
[22] J. Q. You and F. Nori, Phys. Rev. B **68**, 064509 (2003).
[23] J. Q. You, J. S. Tsai, and F. Nori, Phys. Rev. B **68**, 024510 (2003).
[24] I. Chiorescu, P. Bertet, K. Semba, Y. Nakamura, C. J. P. M. Harmans, and J. E. Mooij, Nature (London) **431**, 159 (2004).
[25] J. Q. You and F. Nori, Phys. Today **58**, 42 (2005).
[26] L. D. Landau and E. M. Lifshitz, *Quantum Mechanics (Nonrelativistic Theory)* (Butterworth, Boston, 1991).
[27] S. Flügge, *Practical Quantum Mechanics* (Springer, Berlin, 1999).
[28] M. Patterson and S. Hughes, e-print arXiv:1002.4208v1.
[29] K. Y. Bliokh, Y. P. Bliokh, V. Freilikher, S. Savel'ev, and F. Nori, Rev. Mod. Phys. **80**, 1201 (2008).
[30] D. F. Walls and G. J. Milburn, *Quantum Optics* (Springer, Berlin, 1994).
[31] M. F. Yanik and S. Fan, Phys. Rev. Lett. **92**, 083901 (2004).
[32] M. F. Yanik and S. Fan, Phys. Rev. A **71**, 013803 (2005).
[33] L. Zhou, J. Lu, and C. P. Sun, Phys. Rev. A **76**, 012313 (2007).
[34] F. M. Hu, L. Zhou, T. Shi, and C. P. Sun, Phys. Rev. A **76**, 013819 (2007).
[35] S. Mookherjea, Jung S. Park, Shun-Hui Yang, and Prabhakar R. Bandaru, Nat. Photonics **2**, 90 (2008).
[36] J. Grgić, E. Campaioli, S. Raza, P. Bassi, and N. A. Mortensen, Opt. Quantum Electron. **5**, 10009 (2010).